Time-resolved magnetic circular dichroism spectroscopy of photolyzed carbonmonoxy cytochrome c oxidase (cytochrome aa_3)

Robert A. Goldbeck,* Timothy D. Dawes,* Ólöf Einarsdóttir,* William H. Woodruff,‡ and David S. Kliger*
*Department of Chemistry and Biochemistry, University of California at Santa Cruz, Santa Cruz, California 95064; and ‡Isotope and Structural Chemistry Group (INC-4), Los Alamos National Laboratory, Los Alamos, New Mexico 87545 USA

ABSTRACT Nanosecond time-resolved magnetic circular dichroism (TRMCD) and time-resolved natural circular dichroism (TRCD) measurements of photolysis products of the CO complex of eukaryotic cytochrome c oxidase (CcO-CO) are presented. TRMCD spectra obtained at 100 ns and 10 μs after photolysis are diagnostic of pentacoordinate cytochrome a_3 Fe^{2+}, as would be expected for simple photodissociation. Other time-resolved spectroscopies (UV-visible and resonance Raman), however, show evidence for unusual Fe_{a3}^{2+} coordination after CO photolysis (Woodruff, W. H., Ó. Einarsdóttir, R. B. Dyer, K. A. Bagley, G. Palmer, S. J. Atherton, R. A. Goldbeck, T. D. Dawes, and D. S. Kliger. 1991. *Proc. Nat. Acad. Sci. U.S.A.* 88:2588–2592). Furthermore, time-resolved IR experiments have shown that photodissociated CO binds to Cu_B^+ prior to recombining with Fe_{a3}^{2+} (Dyer, R. B., Ó. Einarsdóttir, P. M. Killough, J. J. López-Garriga, and W. H. Woodruff. 1989. *J. Am. Chem. Soc.* 111:7657–7659). A model of the CcO-CO photolysis cycle which is consistent with all of the spectroscopic results is presented. A novel feature of this model is the coordination of a ligand endogenous to the protein to the Fe axial site vacated by the photolyzed CO and the simultaneous breaking of the Fe-imidazole(histidine) bond.

INTRODUCTION

Cytochrome *c* oxidase (CcO) plays a complex and pivotal role in the biochemistry of respiration. As the terminal oxidase in the oxidative metabolism of aerobic organisms, the resting enzyme accepts electrons from cytochrome *c* and, in its reduced state, binds molecular oxygen and reduces it to water. The free energy released by this redox chemistry is coupled by a mechanism that is not understood to the transfer of protons by the protein across the mitochondrial membrane (1). The proton gradient produced by translocation drives the production of ATP, the energy currency of the cell, by processes within the mitochondria.

In keeping with the complex function of the enzyme, the structure of the protein is also complex and not completely known; therefore, only the features important to understanding the spectroscopy of photodissociable ligand complexes of cytochrome oxidase are briefly summarized here (for reviews, see references 1–3). There are at least four metal centers known to be essential to function, two heme A iron atoms and two copper atoms. Other metals (Zn and Mg) have also been found to be present (4), but their specific roles are unknown. Cytochrome *a* is a hexacoordinate heme A which is axially ligated to two neutral histidine imidazoles and is low spin in both oxidation states ($S = 0$ in the ferrous state, $S = ½$ in the ferric state). Both cytochrome *a* and the nearby Cu_A center are involved in accepting electrons from cytochrome *c* and transferring them to the ligand binding site, which consists of cytochrome a_3 and Cu_B. Cytochrome a_3 is a penta- or hexacoordinate heme A which is axially ligated to a histidine distal to the Cu_B. In the reduced state of the enzyme, the sixth coordination site in cytochrome a_3 can bind typical heme ligands such as O_2, CO, or NO. The resting state of the enzyme is not available to these ligands and shows a strong antiferromagnetic coupling between cytochrome a_3 and Cu_B by an unknown bridging ligand. Cytochrome a_3 is high-spin in the resting enzyme ($S = 5/2$) and in the unliganded reduced form ($S = 2$). As is the case for ligand binding to the protoheme of hemoglobin, binding of a sixth ligand to cytochrome a_3^{2+} causes the ferrous heme to become low spin ($S = 0$).

Many kinetic studies of binding of ligands to the reduced enzyme have employed photolysis of the CO complex to rapidly prepare the unliganded enzyme (5). These "flow-flash" studies have implicitly assumed that photodissociation of CO is itself a kinetically simple process. However, recent time-resolved IR (TRIR) (6) and time-resolved UV-vis absorption spectroscopy (TRUVV) (Einarsdóttir, Ó., P. M. Killough, R. B. Dyer, J. J. López-Garriga, S. M. Hubig, S. J. Atherton, G. Palmer, and W. H. Woodruff, unpublished results) studies have shown that the kinetics of CO photolysis are more complex than was previously believed. In particular, Cu_B^+ was found to function in a "ligand shuttle" that sequestered CO (and perhaps other exogenous ligands such as O_2) as they traveled to and from the heme of cytochrome a_3^{2+}. Furthermore, the rate of cytochrome a_3-CO recombination was found to be slow ($t_{1/2} > 1$ ms) and to depend on light intensity, implying that a photo-

0006-3495/91/07/125/10 $2.00

labile endogenous ligand prevents CO from recombining with the cytochrome a_3^{2+} of the protein as rapidly as is observed in other ligand-binding heme proteins.

To study the coordination of cytochrome a_3 at times greater than several nanoseconds after CO photodissociation, we have applied a recently developed technique for measuring time-resolved magnetic circular dichroism (TRMCD) spectra (7, 8). MCD spectroscopy is sensitive to the spin state of the cytochrome a_3 iron in both oxidation states of cytochrome oxidase (9). Therefore, the correlation of spin state with the axial ligation of the cytochrome a_3 Fe^{2+} allows the TRMCD spectrum to be used as a time-resolved probe of cytochrome a_3 coordination.

In this report we discuss the technique for measuring MCD on a nanosecond timescale, the nature of the TRMCD results, and its implications for models of CcO-CO photolysis. In a preliminary report of the TRMCD of cytochrome oxidase we found that cytochrome a_3 iron goes to a high-spin state within the time resolution of our instrument (several nanoseconds) and stays high spin until CO recombination occurs milliseconds later (10). Here we present detailed experimental evidence which supports this conclusion. This finding implies that the iron (Fea_3^{2+}) is pentacoordinate promptly after CO photolysis, as would be expected for a simple photodissociation. However, the time-resolved resonance Raman (TR^3) spectra also reported suggest that either Fea_3^{2+} remains hexacoordinate after photolysis or that Fe-histidine coordination is lost. Taken all together, the evidence from time-resolved UV-vis, IR, MCD, and RR spectroscopy requires a more complex model in which photodissociation of CO from cytochrome a_3 triggers the binding of an endogenous ligand to the iron of cytochrome a_3 that both displaces the proximal histidine and inhibits CO recombination.

METHOD

TRMCD technique

Natural and magnetic circular dichroism are difficult to measure directly because $\Delta\epsilon = \epsilon_L - \epsilon_R$ is small compared to ϵ_R and ϵ_L. Therefore, rather than measure ϵ_R and ϵ_L directly, the TRMCD technique (7, 8) uses a quasinull, ellipsometric method in which a light beam with slightly elliptical polarization (horizontal axis intensity about 10^4 times the vertical axis intensity) is used to interrogate the circular dichroism of the sample. The elliptically polarized probe light is obtained by passing a beam from the probe source through a horizontal linear polarizer and then through a fused silica plate in which a slight birefringence (1° of retardance, fast axis at ±45° from horizontal) has been induced by the application of a mechanical strain. Passing the beam through a circularly dichroic sample changes the ellipticity of the beam. This change is detected with an analyzing vertical polarizer placed in front of the light detector (Fig. 1). The

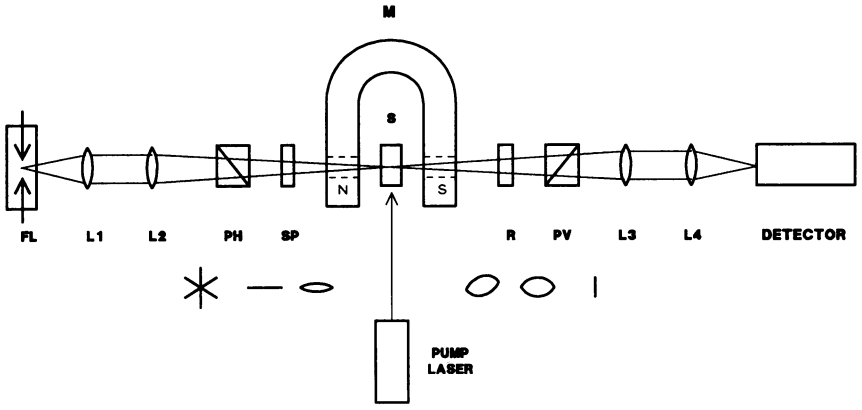

FIGURE 1 Schematic of apparatus used for nanosecond time-resolved MCD measurements. The appropriate harmonic of a pulsed Nd:YAG laser is used for initiating photolysis reactions (frequency doubled to 532 nm in present work). Probe light is generated by a xenon flashlamp (FL), collimated and focused (L1 and L2) through a polarizer (P_H) and strained fused-silica plate (SP) retarder before entering the sample cell (S). The retarder introduces a small amount of elliptical polarization into the probe beam. The sample is placed between the pole faces of a magnet (M) that produces a magnetic field parallel (antiparallel) to the propagation vector of the probe beam. Passing the beam through a magnetically circular dichroic sample changes the eccentricity of the polarization ellipse of the beam, while the Faraday effect of cell windows and solvent rotates the polarization axis of the beam. The Faraday effect is levorotatory (dextrorotatory) for a parallel (antiparallel) magnetic field orientation. The Faraday rotation is cancelled by a compensating rotation provided by a polarization rotator (R), e.g., a sucrose (fructose) solution. The change in elliptical polarization induced in the beam by the sample is determined by a polarizer (P_V) with axis oriented perpendicular to that of P_H. The probe light is recollimated and focused (L3 and L4) into a detection system consisting of a monochromator and photomultiplier, or a spectrograph and optical multichannel analyzer. The figures below the optical track indicate the polarization state of the probe beam at various points along the optical path.

signal measured is

$$S = (I_R - I_L)/(I_R + I_L), \quad (1)$$

where I_R and I_L are the intensity of the probe beam with the strain plate oriented at +45° and −45°, producing right- and left-handed elliptically polarized light, respectively. The circular dichroism, $\Delta\epsilon$, is related to this signal by

$$S = 2.3\Delta\epsilon cz/\delta \quad (2)$$

where c is the concentration in moles/liter, z is the pathlength in centimeters, and δ is the retardance of the strain plate in radians (11).

MCD and natural CD were distinguished by taking measurements with the field of the magnet (JASCO PM-2 permanent magnet, 0.64 Tesla average longitudinal field strength) oriented parallel and antiparallel to the propagation vector of the probe beam (magnetic field points from north to south pole). The difference and sum of the two signals, divided by two, yields the MCD and natural CD, respectively. The magnet was mounted on a horizontal translation stage which allowed the magnet to be removed or reversed in field orientation without disturbing the sample cell. As a check of the technique and the spectral corrections described below, CD spectra obtained in the presence of the magnetic field were checked for consistency with CD spectra obtained at zero magnetic field.

Instrumentation

The sample was photolysed with a 532-nm, 20-mJ, 7-ns pulse from a frequency-doubled Nd:YAG laser DCR-11 (Quanta-Ray, Mountain View, CA). The probe source was a 5-μs duration xenon flashlamp FX-193 (EG&G, Salem, MA). TRMCD spectra were obtained by detecting the probe beam with an optical multichannel analyzer (OMA) instrument consisting of a Monospec 27 (Jarrell-Ash) spectrograph (250-μm slit, 150 g/mm), EG&G 1420 gated detector with an EG&G 1304 pulse amplifier supplying 120-ns and 2-μs gates for measurements at the 100-ns and 10-μs delay times, respectively, and an EG&G 1461 detector interface. Kinetic measurements at single wavelengths were made with a monochromator (MP-1018B Pacific Precision Instruments, Concord, CA) and photomultiplier (9876QB EMI-GENCOM) whose output was recorded with a programmable digitizer (7912AD; Tektronix, Inc., Beaverton, OR.)

Signal-to-noise in TRMCD

Conventional MCD instruments achieve the signal-to-noise ratio necessary to measure a $\Delta\epsilon$ that is only $10^{-4}\epsilon$ by AC modulating the probe beam polarization and detecting the AC component of the transmitted light with a phase-locked amplifier. This technology is inherently limited by the physical constraints of the optoacoustic modulator. The maximum time resolution of kinetic MCD measurements has thus been limited to the millisecond regime. The TRMCD technique achieves a signal-to-noise improvement over a direct measurement of $\Delta\epsilon$ by detecting a change in intensity that is 100 times larger (at 1° retardance) than in a direct measurement (8). This puts much less demand on the stability of the lamp and detector. Furthermore, photon shot noise can be reduced in TRMCD by the use of much brighter light sources, e.g., xenon flashlamps, than are used in conventional instruments. In principle, there is no shot noise advantage to this technique over a direct measurement using circularly polarized light from a source of the same intensity because the beam is attenuated by 10^{-4} in the TRMCD measurement. Because the shot noise increases as the inverse square root of the intensity, this just offsets the 10^2 increase in signal. In practice, however, shot noise is reduced in TRMCD measurements by the use of light sources which are much brighter for the short duration of the measurement. This yields a higher signal-to-noise ratio than would be possible in a direct measurement. Altogether, the signal-to-noise advantages of the TRMCD technique make it possible to measure MCD with nanosecond time resolution (7).

Canceling the effect of Faraday rotation

A complication of the ellipsometric TRMCD technique that does not arise in conventional MCD measurements, which are made with circularly polarized light, is a rotation of the polarization axis of the elliptically polarized probe beam by the Faraday effect of the sample cell and solvent in the applied magnetic field. The rotation produced in the beam after traveling through 8 mm of water and quartz immersed in a 0.64-Tesla magnetic field is large (several degrees) compared with the strain plate retardance. This rotation must be compensated in order to obtain a TRMCD measurement. The Faraday rotation produced by the dissolved sample itself is small compared with the strain plate retardance and can be neglected (8).

The simplest technique for canceling this rotation, which was used for kinetic MCD measurements at a single wavelength, is to rotate the analyzing polarizer by an angle equal to the Faraday angle at the detected wavelength. This is not useful, however, for measurements of time-resolved MCD spectra with OMA detection because the Faraday rotation angle varies with wavelength (magnetic optical rotatory dispersion [MORD]). This MORD of the cell and solvent was canceled with a sucrose or fructose solution placed before the analyzing polarizer for the parallel and antiparallel field orientations, respectively. An entire spectrum can be taken with OMA detection using this method because the ORD bandshapes for sucrose and fructose match the MORD band shape of the water-filled quartz cell to within 0.5% over the 350–650 nm wavelength region. Fructose is mutarotatory; therefore, care must be taken when preparing solutions of fructose to allow enough time, ~48 h, for its anomers to equilibrate. In general, both the MORD and ORD of transparent materials have an approximate $1/\lambda^2$ dependence on wavelengths far from absorption bands. This fact makes the excellent coincidence of ORD and MORD found in this case appear less surprising. The ORD of another highly soluble, optically active substance, L-proline, for example, was also found to give satisfactory (within 5%) cancelation of MORD over the same wavelength region. An alternative method, though more technically difficult, for canceling Faraday rotation would be to pass the beam through a second cell containing solvent in a matching magnetic field of opposite polarity. An electromagnet is required because the second, canceling field must be adjustable.

Smoothing and photolysis yield corrections applied to spectral data

The spectral resolution of spectra taken with the OMA was limited by the spectrograph slit width to 1.6 nm. Because this encompasses several bins of the detector array (0.6 nm/bin), a simple box smoothing was applied to spectral data to maximize signal to noise within the available resolution. A box half-width of 1.8 nm was used for wavelengths below 500 nm and a half-width of 4.2 nm was applied to the wavelengths above 500 nm. This box averaging gave results that were essentially identical to spectra obtained by applying a 25 point Savitzky-Golay cubic polynomial fitting algorithm to the data.

The spectra presented were corrected for nonflat baselines and for the effects of extinction, as explained below. The spectra of transient species were corrected for incomplete photolysis by subtracting the

spectrum of the unphotolyzed fraction from the observed signal, and dividing by the photolysis yield. This correction is shown in the following equation:

$$T(\lambda) = [T_0(\lambda) - (1 - \phi)U(\lambda)]/\phi, \quad (3)$$

where $T(\lambda)$ is the corrected time-resolved spectrum, $T_0(\lambda)$ is the observed time-resolved spectrum, $U(\lambda)$ is the spectrum of the unphotolyzed complex, and ϕ is the fractional photolysis yield. Because ϕ was approximately 0.9, this correction was on the order of 10%.

Correction of TRMCD spectra for imperfect extinction

Because the TRMCD technique is a quasinull method (the light intensity transmitted by a 1° retarder between crossed polarizers is about 10^{-4} of incident intensity), excellent extinction is required from the combination of the crossed polarizers and the optics between them. The extinction of the probe beam intensity by the crossed Glan-Taylor prisms used in the experiment was $\sim 10^{-6}$. Loss of extinction due to light scattering by the filtered sample and sample cell window strain was sufficiently small that the extinction ratio remained $< 10^{-5}$. The largest contribution to decreased extinction was due to the inhomogeneity of the magnetic field, which raised the extinction ratio to 10^{-5} by inducing a spread in Faraday rotation angles across the probe beam cross-section. (Although the average Faraday rotation was canceled by applying the measures described above, both undercanceling near the edges and overcanceling at the center of the beam will give rise to excess light transmission.) The decrease of extinction due to cell imperfections, light scattering, and the cross-sectional variation in Faraday rotation will attenuate the signal as it is calculated in Eq. 1. This attenuation ($\sim 10\%$ in the Soret band) was corrected for in the present study by employing the form shown in Eq. 4 in which these contributions have been subtracted from I_R and I_L:

$$S = (I_R - I_L)/(I_R + I_L - 2I_X), \quad (4)$$

where I_X is the intensity of light transmitted with the strain plate retarder removed. The validity of this correction was confirmed by comparing natural CD spectra obtained from summing the TRMCD signals for opposite field polarities with TRCD spectra obtained at zero field. Zero-field and high-field TRCD spectra calculated from Eq. 1 differed by $\sim 10\%$ in magnitude, whereas spectra calculated from Eq. 4 were identical within the noise.

Linear birefringence artifacts

The possibility of linear birefringence (LB) artifacts due to photoselection by the linearly polarized laser must be considered because the rotational reorientation time of the protein (hundreds of nanoseconds) is comparable to the time scale being probed (12). Linear birefringence artifacts in TRMCD measurements can be minimized when exciting the sample with a horizontally polarized laser beam by propagating the pump and probe beams at 90° to each other in the horizontal plane (13). The TRMCD and TRCD data presented here were taken with this excitation geometry. The absence of appreciable LB artifacts was confirmed by the close resemblance of the transient spectra obtained to the literature MCD and CD spectra of corresponding equilibrium species (9, 14).

Sample preparation

Cytochrome oxidase (cytochrome aa_3, CcO) was prepared from fresh bovine heart muscle by the method of Yoshikawa et al. (15) with modifications to be described elsewhere (Einarsdóttir, Ó., P. M. Killough, R. B. Dyer, J. J. López-Garriga, S. M. Hubig, S. J. Atherton, G. Palmer, and W. H. Woodruff, unpublished results). The reduced enzyme was obtained by deoxygenating the resting, oxidized enzyme with alternating cycles of vacuum and Ar gas, followed by the addition of a small excess of dithionite. 15–20 min were allowed to obtain the fully reduced enzyme. The complex of the reduced enzyme with carbon monoxide was obtained by passing 1 atm CO over the reduced enzyme solution for 45 min. Samples used in the TRMCD measurements were 8–20 μM in protein.

RESULTS

TRMCD spectra

Photolysis of the carbonmonoxy complex of reduced cytochrome aa_3 (CcO-CO) promptly yields a species whose TRMCD spectrum resembles the MCD spectrum of the equilibrium unliganded enzyme. This can be seen in Fig. 2, where Soret region TRMCD spectra taken with OMA gates starting 100 ns and 10 μs after laser photolysis are displayed. (All spectra shown in this paper are on a per mol enzyme basis.) Both curves show the doubling in peak-to-trough amplitude and blue-shift relative to the MCD of the complex that is seen in the spectrum of the unliganded enzyme. The TRMCD in the visible α band region, shown in Fig. 3, is also similar to the MCD of the unliganded enzyme.

Only small differences in Soret band position, width, and intensity distinguish the 100-ns and 10-μs transient species and the equilibrium unliganded enzyme. The 10-μs TRMCD band maximum at 448 nm is very close to that of the unliganded enzyme (448 nm), whereas the band maximum (449 nm) of the TRMCD spectrum taken at the shorter, 100-ns time interval, lies between the liganded (452 nm) and unliganded maxima. The intensity of the 100-ns peak is slightly reduced from the

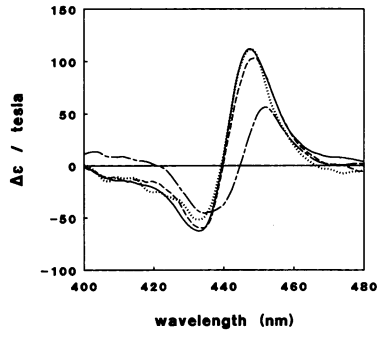

FIGURE 2 Soret region TRMCD spectra at 100–220 ns (-----) and 10–12 μs (·····) after photolysis of 8 μM CcO-CO. Shown for comparison are the equilibrium MCD of CcO-CO (— - —) and reduced CcO (———). MCD is calculated from Eqs. 2 and 4. Magnetic field strength is 0.64 T.

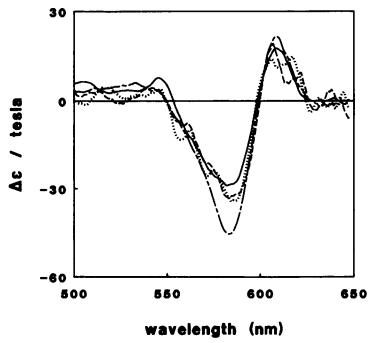

FIGURE 3 α band TRMCD spectra at 100–220 ns (-----) and 10–12 μs (·····) after photolysis of 8 μM CcO-CO. Shown for comparison are the equilibrium MCD of CcO-CO (— - —) and reduced CcO (———). MCD is calculated from Eqs. 2 and 4. Magnetic field strength is 0.64 T.

10-μs and unliganded maxima. The transient MCD spectra are also distinguished from the unliganded MCD spectrum by their slightly smaller bandwidths.

It is desirable to focus on the changes occurring in the Soret region MCD spectrum of individual cytochrome a_3^{2+}, the site of ligand binding. The MCD spectrum of cytochrome a_3^{2+} can be isolated from the spectrum of the full enzyme by taking the difference spectrum between the deliganded enzyme and the CO complex because, as shown by Babcock et al. (9), the Soret MCD spectrum of the CO complex is almost entirely contributed by the non-ligand-binding cytochrome *a*. The MCD spectrum of the latter appears to be independent of the ligation state of cytochrome a_3. The difference spectra in Fig. 4 show the MCD of the photolyzed complex and the unliganded enzyme after the constant background of the cytochrome *a* spectrum has been subtracted out. The positive MCD peak near 445 nm is very similar in the photolyzed and unliganded species. Most of the small differences in bandshape and position that were seen in the spectra in Fig. 2 correspond in Fig. 4 to intensity differences of weak transitions occurring at energies just below that of the strong Soret band of cytochrome a_3. These may be due to ligand-metal charge transfer bands. Fig. 4 emphasizes the lower intensity of the Soret MCD maxima of the enzyme at 100 ns after photolysis as compared to the 10-μs photolysis product and the steady-state unliganded enzyme. Nevertheless, the TRMCD spectra of cytochrome a_3^{2+} taken at 100 ns and 10 μs after photodissociation are clearly similar to the MCD of the unliganded species.

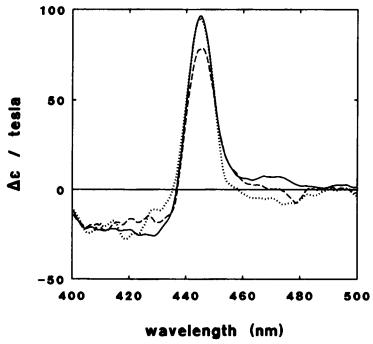

FIGURE 4 Soret region TRMCD spectra of individual cytochrome a_3^{2+} at 100–220 ns (-----) and 10–12 μs (·····) after photolysis of CcO-CO. Shown for comparison is the equilibrium MCD of cytochrome a_3^{2+} (———). The MCD of cytochrome a_3^{2+} is calculated by subtracting the MCD spectrum of the CO complex from the spectrum of the deliganded enzyme (see text).

The appearance of unliganded-like TRMCD after photolysis is instantaneous within the time resolution of our apparatus (several nanoseconds). The kinetics of the change in MCD measured at 445 nm (Fig. 5) shows a sharp increase upon photolysis that is consistent with the difference between unliganded and liganded spectra shown in Fig. 2. The small difference in Δε at 445 nm for the 100-ns and 10-μs TRMCD spectra in Fig. 2 indicates that there is a small growing in of the MCD signal shown in Fig. 5. The time span of the trace in Fig. 5, ~1 μs, is too short, however, for this small change to become apparent over the noise.

TRCD spectra

The major Soret peaks in the TRCD spectrum of the photolyzed complex (444 nm) and the steady-state CD spectrum of the unliganded enzyme (445 nm) shown in Fig. 6 are narrowed and red-shifted relative to the peak

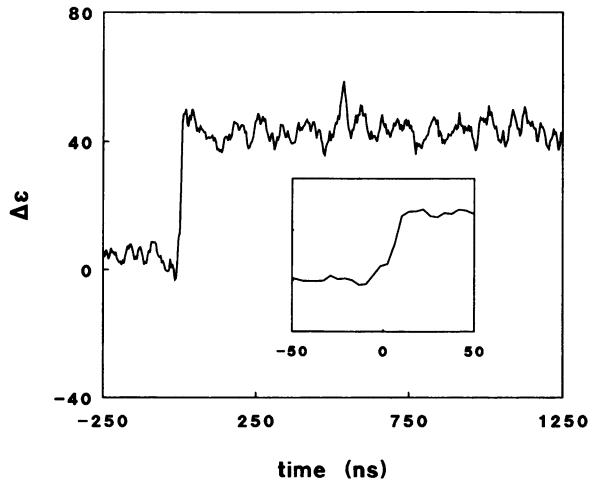

FIGURE 5 Kinetic TRMCD trace of CcO-CO photolysis monitored at 445 nm. Inset shows (instrument-limited) risetime of signal. Zero of abscissa is arbitrary. Magnetic field strength is 0.64 T.

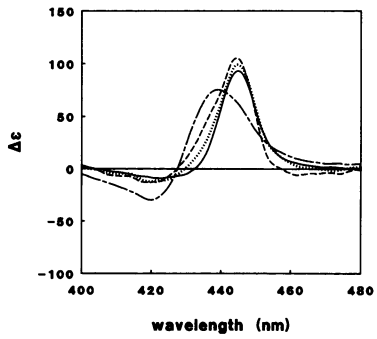

FIGURE 6 Soret region TRCD spectra at 100–220 ns (-----) and 10–12 μs (·····) after photolysis of 8 μM CcO-CO. Shown for comparison are the equilibrium CD of CcO-CO (— - —) and reduced CcO (———). CD is calculated from Eqs. 2 and 4.

(439 nm) in the CD spectrum of the CO-complex. The TRCD also shows a prompt change in the Soret region upon photolysis, as shown in Figs. 6 and 7. The sharp decrease upon photolysis seen in the kinetic trace of CD at 435 nm is consistent with the difference between the CD spectra of the unliganded/transient species and the CO complex at that wavelength. The α band CD, which contains a small positive peak near 610 nm, is not shown as it does not change appreciably with photolysis. As was the case for the MCD spectra, the TRCD and unliganded CD spectra are clearly similar, although the short-time Soret band TRCD spectrum is intermediate in band position and shape between the reduced enzyme and the CO complex.

DISCUSSION

MCD of equilibrium CcO and CcO-CO

Previous studies of reduced cytochrome *c* oxidase and its complexes (9), as well as model heme complexes (16),

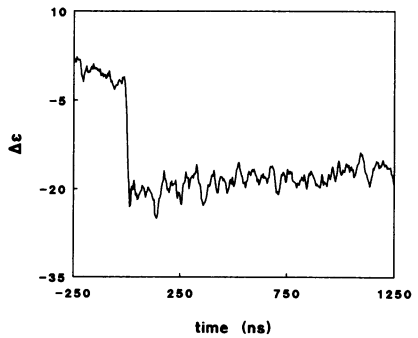

FIGURE 7 Kinetic TRCD trace of CcO-CO photolysis monitored at 435 nm. Zero of abscissa is arbitrary.

have established the sensitivity of the Soret band MCD to the spin state of the cytochrome a_3 iron. This sensitivity is seen in the doubling of peak-to-trough MCD amplitude in the Soret band of the unliganded enzyme relative to the complex which accompanies the change in spin state of Fe_{a_3}. As mentioned above, low-spin cytochrome a_3^{2+} makes very little contribution to the MCD observed near 445 nm for the liganded enzyme; most of the intensity at this wavelength has been assigned to the A-term (derivativelike bandshape) MCD of cytochrome a^{2+}. In contrast, cytochrome a_3^{2+} is pentacoordinate and high-spin in uncomplexed CcO, and its contribution to the MCD of CcO at 445 nm is dominant over that of cytochrome a^{2+}, which remains hexacoordinate and low-spin.

The dramatic increase in MCD intensity for the cytochrome a_3^{2+} upon CO photodissociation is due to the change from diamagnetic to paramagnetic $Fe_{a_3}^{2+}$ that occurs when coordination to the ligand is lost. The introduction of spin degeneracy in the ground electronic state of the iron–porphyrin complex gives rise to C-term MCD. In general, given identical magnetic and electronic transition dipoles, C-term MCD (which is inversely proportional to temperature) dominates over A-term MCD when the molecular bandwidth ($h\Delta\nu$) is larger than the thermal energy (kT) (17), as is the case here. Thus, the change in ligand coordination at the cytochrome a_3^{2+} site of the protein is correlated with a qualitative change in the nature of the Soret band MCD.

Comparison with other time-resolved spectroscopies

The initial photophysical and photochemical events of photodissociation of CO from cytochrome a_3 Fe^{2+} are probably complete within a picosecond, in analogy to hemoglobin (18). These subpicosecond events include the spin-state change responsible for the sharp change observed in the MCD of the Soret band. The TRMCD results of the present study show that the MCD spectrum expected for pentacoordinate, high-spin $Fe_{a_3}^{2+}$ does appear within the time resolution of our apparatus and remains until CO recombines with $Fe_{a_3}^{2+}$ milliseconds later.

The events after the initial photodissociation of CO-Fe_{a_3} have been followed by a variety of time-resolved spectroscopies in addition to TRMCD. TRUVV has been used to study CcO-CO photolysis on the picosecond to kilosecond time scales (Einarsdóttir, Ó., P. M. Killough, R. B. Dyer, J. J. López-Garriga, S. M. Hubig, S. J. Atherton, G. Palmer, and W. H. Woodruff, unpublished results). The most dramatic feature in the UV-vis spectrum, after the initial effect of photolysis on the Soret band, is the growing in of absorbance at 610 nm in

the α band with a ~10-ps time constant and then a loss of this absorbance gain with a 1-μs time constant. The latter feature is probably correlated with the small evolution on a comparable timescale seen in the TRMCD and TRCD spectra. The other interesting feature seen in TRUVV is the photoacceleration of the overall recombination rate. Recombination was seen to proceed with a pseudo–first order rate constant of 84 s^{-1} at low light levels, increasing to 108 s^{-1} when the probe intensity was increased 60-fold. A similar variation of the TRMCD probe light intensity showed no evidence for photolability. This negative result is probably due to the lower light flux, when integrated over the recombination lifetime, of the microsecond flash used in the TRMCD experiment as compared with the continuous wave lamp used in the TRUVV measurement. TRIR (6) shows the appearance after CcO-CO photolysis of a Cu-CO vibrational peak at 2,061 cm^{-1} that decays with a 1.5-μs half-life. This result directly establishes the binding of photolyzed CO to Cu_B^+ at room temperature. It had been previously established by FTIR that, in mitochondria, photodissociated CO binds to Cu_B at low temperatures (19). Unfortunately, Cu_B^+ appears to be spectroscopically silent in the near UV-visible region and is not clearly visible in the TRMCD and TRCD spectra. The TR^3 (*vide supra*) spectrum taken 200 ns after photolysis shows a loss of intensity of the Fe-N(imidazole) stretch at 223 cm^{-1}. This RR line is considered a marker for Fe coordination, and indicates that either Fe_{a_3} is hexacoordinate or that it has lost coordination to the imidazole of the proximal histidine after photolysis. The TRMCD results are consistent with the latter interpretation.

Kinetic models of CO photolysis and recombination

A classical model (model I) of hemeprotein-CO photolysis/recombination, modified to include the binding of photodissociated CO to Cu_B now established by TRIR in CcO, is shown in Scheme I. A similar model has been presented before for CcO–CO (6). The negligible geminate recombination yield of CcO-CO implies that photodissociated CO quickly binds to Cu_B^+ (**3** to **2** in Scheme I), before it can recombine with Fe (the latter process is expected to require ~100 ns, in analogy to hemoglobin). This sets a lower bound of $\sim 10^9$ s^{-1} on the order of magnitude of k_{-2}. Both k_{-1} and k_2 are determined from the half-life for CO release by Cu_B, as directly measured by TRIR. k_1 is the pseudo first-order rate constant for CcO-CO heme pocket recombination for an enzyme solution under 1 atm of CO. In this model, the very slow (10^{-2}–10^{-1} s) observed recombination time for Fe_{a_3}-CO arises as a product of the microsecond Cu-CO off rate and the small percentage of geminate dissociative states that succeed in recombining with Fe.

$$[Fe_{a_3},Cu_B] + CO \underset{k_{-1}}{\overset{k_1}{\rightleftharpoons}} [Fe_{a_3},Cu_B\text{-}CO] \underset{k_{-2}}{\overset{k_2}{\rightleftharpoons}}$$
$$\mathbf{1} \qquad\qquad \mathbf{2}$$

$$[Fe_{a_3},CO,Cu_B] \underset{h\nu}{\overset{k_3}{\rightleftharpoons}} [Fe_{a_3}\text{-}CO,Cu_B]$$
$$\mathbf{3} \qquad\qquad \mathbf{4}$$

Scheme I

Whereas the classical model of Fe-CO photodissociation (modified to include Cu_B^+-CO binding) is consistent with the TRMCD of cytochrome a_3, it is inadequate to explain the TR^3 and TRUVV results (10) which indicate that the coordination of $Fe_{a_3}^{2+}$ undergoes additional transient changes subsequent to CO photodissociation. In particular, the increase in CO recombination rate that accompanies increased probe light intensity in the TRUVV study implies that a photolabile, endogenous ligand (L) occupies the Fe coordination site vacated by CO. If the rate limiting step for CO recombination is the thermal dissociation of L from Fe, then photolysis of the Fe-L bond would actually increase the CO recombination rate. Further evidence for unusual cytochrome a_3 coordination is found in the TR^3 spectrum, as discussed above. An interpretation that is consistent with these results and with the TRMCD results is that subsequent to CO photolysis binding of CO to Cu_B displaces L from Cu_B and triggers L to occupy the vacant Fe site distal to the histidine. Furthermore, binding of L to Fe simultaneously forces the dissociation of the histidine imidazole, leaving the iron pentacoordinate at all times after CO photolysis, as indicated by the TRMCD results. A schematic picture of this model (model II) of CO photolysis is shown in Fig. 8.

The slow observed recombination time is explained in model II as a product of the slow thermal rate of Fe-L bond scission in **2**, Fig. 8, and a 1:10 equilibrium between species **2** and **1**. Model II incorporates the photoenhancement of CO recombination observed in the TRUVV study as a photolability of the Fe-L bond in **2**. If Fe-L bond scission is the rate-limiting step for recombination, then **4** must efficiently recombine to give **5**, the stable complex. However, geminate recombination is not observed after CO photodissociation; therefore, **4** cannot be the geminate dissociative state formed after photolysis. Accordingly, the geminate state is shown as **4′**, in which CO and the heme pocket are depicted with excess energy left over from photolysis. Molecular dynamics simulations (20) and picosecond resonance Raman spectroscopy (21) have shown that the energy of a 532 nm photon, minus the Fe-CO bond dissociation energy, is sufficient to raise the temperature of the photolyzed heme by ~200 K. This excess heat is transferred to the surrounding protein solvent with a 30-ps time constant,

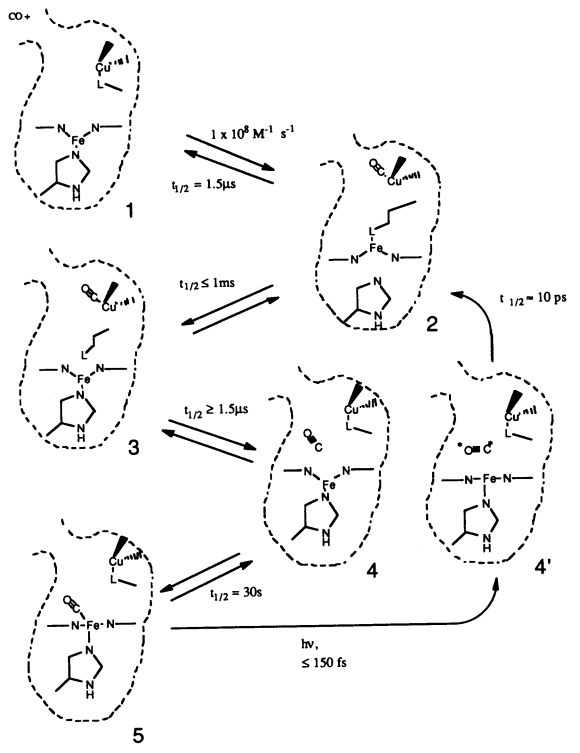

FIGURE 8 Schematic of model II of CcO-CO photolysis and recombination kinetics. Model II is consistent with all spectroscopic observations to date.

where it appears as excess vibrational energy of the contacting protein residues, and rotational and translational energy of the CO (subpicosecond IR of hemoglobin shows that photodissociated CO is vibrationally unexcited [22]). It is postulated that before the pocket thermalizes with the rest of the protein, the activated CO displaces L from Cu_B much more efficiently than does the thermalized CO in **4**, preventing geminate recombination. Whereas the replacement of L for imidazole on Fe is shown as proceeding in concert in the step from **4'** to **2**, the sequential pathway **4'** → **3** → **2** is also possible because **3** and **2** are probably in a rapid equilibrium favoring formation of **2**.

Two questions raised by model II are: (*a*) What is the identity of the endogenous ligand L? (*b*) How can distal bonding of L to pentacoordinate Fe_{a_3} displace the proximal histidine? While these questions cannot yet be answered, our preliminary report (10) considered candidates for L such as residues nearby on the protein and the unsaturated farnesyl side chain of the heme A. Because there seems to be no precedent for an electronic explanation for the postulated displacement reaction, it was concluded that the possibility of unusual steric effects offered by the long chain of the farnesyl moiety makes it the most promising candidate.

Cytochrome a_3 heme pocket relaxation

The photolysis of ligands from hemeproteins generally triggers subsequent relaxations in tertiary and quaternary structure as the protein slowly accommodates to the sudden change from a liganded to a deliganded heme pocket. The Fe-CO bond is broken in less than a picosecond, while the large scale motion of protein residues and chains needed to stabilize the new electronic structure of the heme requires nanoseconds to microseconds. The coupling of heme structure to the organization of the heme pocket and the rest of the protein is thought to mainly reside in the heme-Fe-histidine imidazole bond angle (23 and references therein).

The photolysis of carbon monoxide from hemoglobin and myoglobin initiates a relaxation process in the tertiary structure of these proteins that is observed on a 0.7–0.9 μs timescale (24, 25). Similarly, TR^3 of CcO-CO also shows evidence for a microsecond timescale reorganization of protein structure around the heme (23). The CcO-CO TRMCD and TRCD spectra obtained in the present study show subtle spectral evolution on a similar timescale. The small shifts in the 100-ns TRMCD and TRCD spectra relative to the 10-μs spectra may be due to a protein relaxation process with a 10^6–10^7 s^{-1} rate constant. The movement of protein helices associated with hemepocket relaxation would be expected to influence the TRCD spectrum. Similarly, changes in the orientation of ligand L associated with relaxation could conceivably influence the TRMCD spectrum, as could a change in orientation or hydrogen bonding of the heme formyl group (26).

An alternate explanation is that these subtle changes are due to ligation changes at the heme. In particular, spectral changes associated with a 10^6 s^{-1} rate constant could be assigned to the decay of **2** to **1** in Fig. 8. In this scenario, the replacement of L on Fe_{a_3} by histidine would account for the small changes observed in TRMCD and TRCD bandshapes and positions. This question can be further investigated by examining the MCD of model compounds containing heme with 1,2-dimethylimidazole and an olefin side chain.

SUMMARY CONCLUSIONS

TRMCD spectroscopy was found to be well suited to following photolysis-initiated spin state changes with

nanosecond time resolution in the carbonmonoxy complex of cytochrome *c* oxidase. Furthermore, the TRMCD spectra gave definitive information about the extent of axial ligand coordination to the cytochrome a_3 iron subsequent to CO photolysis. This information proved to be complementary to the information provided by other time-resolved spectroscopic techniques, such as TRIR, TRUVV, and TR[3]. We have presented a model of CO photodissociation and recombination that is consistent with all the spectroscopic results, although it is clear that more information is needed to answer the questions raised by model II. This study points to the importance of TRMCD spectroscopy, applied in conjunction with other spectroscopic techniques, in providing the complementary information needed to assemble a detailed mechanistic picture of hemeprotein function.

It is possible that the shuttling of ligands between Fe_{a_3} and Cu_B observed in these studies may play a role in the physiological function of CcO. The results obtained for CO may be applicable to the interaction of O_2 with the reduced protein in the redox cycle. It is also possible that shuttling of the endogenous ligand L may have a physiological role by providing a gating mechanism for the pumping of protons by the protein. This shuttling must be considered when interpreting the results of flow-flash experiments that rely on photolysis of the CO complex to rapidly provide unliganded enzyme.

A TRMCD study of the photolysis of the CO complex of a bacterial cytochrome oxidase, cytochrome ba_3, is currently in progress. Evidence for a similar ligand shuttle mechanism in this enzyme comes from IR (19) and TRUVV spectral results. In particular, evidence for a photolabile endogenous ligand (L) coordinating to Fe_{a_3} after CO photolysis is even stronger in this protein than in cytochrome aa_3, yet we find the same prompt appearance of high-spin state for the iron (Goldbeck, R. A., T. D. Dawes, Ó. Einarsdóttir, D. B. O'Connor, J. A. Fee,and D. S. Kliger, unpublished results).

Financial support for this work was provided by the National Institutes of Health, grants GM-38549 (Dr. Kliger) and DK-36263 (Dr. Woodruff).

Received for publication 18 November 1990 and in final form 11 March 1991.

REFERENCES

1. Chan, S. I., and P. M. Li. 1990. Cytochrome *c* oxidase: understanding nature's design of a proton pump. *Biochemistry.* 29:1–12.
2. Wikström, M., M. Saraste, and T. Penttilä. 1985. Relationships between structure and function in cytochrome oxidase. *In* The Enzymes of Biological Membranes. Vol. 4. Bioenergetics of Electron and Proton Transport. A. N. Martonosi, editor. Plenum Publishing Corp., New York. 111–148.
3. Scott, R. A. 1989. X-Ray absorption spectroscopic investigations of cytochrome *c* oxidase structure and function. *Annu. Rev. Biophys. Biophys. Chem.* 18:137–158.
4. Einarsdóttir, Ó. and W. S. Caughey. 1985. Bovine heart cytochrome *c* oxidase preparations contain high affinity binding sites for magnesium as well as for zinc, copper, and heme iron. *Biochem. Biophys. Res. Commun.* 129:840–847.
5. Hill, B. C., C. Greenwood, and P. Nicholls. 1986. Intermediate steps in the reaction of cytochrome oxidase with molecular oxygen. *Biochim. Biophys. Acta.* 853:91–113.
6. Dyer, R. B., Ó. Einarsdóttir, P. M. Killough, J. J. López-Garriga, and W. H. Woodruff, 1989. Transient binding of photodissociated CO to Cu_B^+ of eukaryotic cytochrome oxidase at ambient temperature. Direct evidence from time-resolved infrared spectroscopy. *J. Am. Chem. Soc.* 111:7657–7659.
7. Goldbeck, R. A., T. D. Dawes, S. J. Milder, J. W. Lewis, and D. S. Kliger. 1989. Measurement of magnetic circular dichroism (MCD) on a nanosecond timescale. *Chem. Phys. Lett.* 156:545–549.
8. Kliger, D. S., J. W. Lewis, and R. A. Goldbeck. 1989. Time-resolved circular dichroism spectroscopy. *SPIE.* 1057:26–33.
9. Babcock, G. T., L. E. Vickery, and G. Palmer. 1976. Electronic state of heme in cytochrome oxidase. I. Magnetic circular dichroism of the isolated enzyme and its derivatives. *J. Biol. Chem.* 251:7907–7919.
10. Woodruff, W. H., Ó. Einarsdóttir, R. B. Dyer, K. A. Bagley, G. Palmer, S. J. Atherton, R. A. Goldbeck, T. D. Dawes, and D. S. Kliger. 1991. Nature and functional implications of the cytochrome a_3 transients after photodissociation of CO-cytochrome oxidase. *Proc. Natl. Acad. Sci. USA.* 88:2588–2592.
11. Lewis, J. W., R. F. Tilton, C. M. Einterz, S. J. Milder, I. D. Kuntz, and D. S. Kliger. 1985. New technique for measuring circular dichroism changes on a nanosecond time scale. Application to (carbonmonoxy)myoglobin and (carbonmonoxy)hemoglobin. *J. Phys. Chem.* 89:289–294.
12. Einterz, C. M., J. W. Lewis, S. J. Milder, and D. S. Kliger, 1985. Birefringence effects in transient circular dichroism measurements with applications to the photolysis of carbonmonoxyhemoglobin and carbonmonoxymyoglobin. *J. Phys. Chem.* 89:3845–3853.
13. Björling, S. C., R. A. Goldbeck, S. J. Milder, J. W. Lewis, and D. S. Kliger. 1991. Analysis of optical artifacts in ellipsometric measurements of time-resolved circular dichroism. *J. Phys. Chem.* In press.
14. Tiesjema, R. H., and B. F. Van Gelder. 1974. Biochemical and biophysical studies on cytochrome *c* oxidase. XVI. Circular dichroic study of cytochrome *c* oxidase and its ligand complexes. *Biochim. Biophys. Acta.* 347:202–214.
15. Yoshikawa, S., M. G. Choc, M. C. O'Toole, and W. S. Caughey. 1977. An infrared study of CO binding to heart cytochrome *c* oxidase and hemoglobin A. *J. Biol. Chem.* 252:5498–5508.
16. Carter, K., and G. Palmer. 1982. Models of the two heme centers in cytochrome oxidase. The optical properties of cytochrome *a* and a_3. *J. Biol. Chem.* 257:13507–13514.
17. Sutherland, J. C., and B. Holmquist. 1980. Magnetic circular dichroism of biological molecules. *Annu. Rev. Biophys. Bioeng.* 9:293–326.

18. Martin, J.-L., A. Migus, C. Poyart, Y. Lecarpentier, R. Astier, and A. Antonetti. 1983. Femtosecond photolysis of CO-ligated protoheme and hemoproteins: appearance of deoxy species with a 350-fsec time constant. *Proc. Natl. Acad. Sci. USA.* 80:173–178.

19. Einarsdóttir, Ó., P. M. Killough, J. A. Fee, and W. H. Woodruff. 1989. An infrared study of the binding and photodissociation of carbon monoxide in cytochrome ba_3 from *Thermus thermophilus*. *J. Biol. Chem.* 264:2405–2408.

20. Henry, E. R., W. A. Eaton, and R. M. Hochstrasser. 1986. Molecular dynamics simulations of cooling in laser excited heme proteins. *Proc. Natl. Acad. Sci. USA.* 83:8982–8986.

21. Petrich, J. W., and J. L. Martin. 1989. Ultrafast absorption and Raman spectroscopy of hemeproteins. *Chem. Phys.* 131:31–47.

22. Anfinrud, P. A., C. Han, and R. M. Hochstrasser. 1989. Direct observation of ligand dynamics in hemoglobin by subpicosecond infrared spectroscopy. *Proc. Natl. Acad. Sci. USA.* 86:8387–8391.

23. Findsen, E. W., J. Centeno, G. T. Babcock, and M. R. Ondrias. 1987. Cytochrome a_3 hemepocket relaxation subsequent to ligand photolysis from cytochrome oxidase. *J. Am. Chem. Soc.* 109:5367–5372.

24. Friedman, J. M., D. L. Rousseau, and M. R. Ondrias. 1982. Time-resolved resonance Raman studies of hemoglobin. *Annu. Rev. Phys. Chem.* 33:471–491.

25. Hofrichter, J., J. H. Sommer, E. R. Henry, and W. A. Eaton. 1983. Nanosecond absorption spectroscopy of hemoglobin: elementary processes in kinetic cooperativity. *Proc. Natl. Acad. Sci. USA.* 80:2235–2239.

26. Goldbeck, R. A. 1988. Sign variation in the magnetic circular dichroism spectra of π-substituted porphyrins. *Acc. Chem. Res.* 21:95–101.